



A Comparison of Different Guidance Schemes for a Direct Fire Rocket With a Pulse Jet Control Mechanism

**by Thanat Jitpraphai, Bradley Burchett,
and Mark Costello**

ARL-CR-493

April 2002

prepared by

Thanat Jitpraphai, Bradley Burchett, and Mark Costello
Department of Mechanical Engineering
Oregon State University
Corvallis, OR 97331

under contract

DAAD17-01-P-1038

Army Research Laboratory

Aberdeen Proving Ground, MD 21005-5066

ARL-CR-493

April 2002

A Comparison of Different Guidance Schemes for a Direct Fire Rocket With a Pulse Jet Control Mechanism

**Thanat Jitpraphai, Bradley Burchett, and Mark
Costello**

Oregon State University

prepared by

Thanat Jitpraphai, Bradley Burchett, and Mark Costello
Department of Mechanical Engineering
Oregon State University
Corvallis, OR 97331

under contract

DAAD17-01-P-1038

Approved for public release; distribution is unlimited.

Abstract

Compared to gun launch ammunition, uncontrolled direct fire atmospheric rockets are terribly inaccurate, to the point where they are used most effectively on the battlefield as area weapons. Dispersion characteristics can be dramatically improved by outfitting the rocket with a suitable control mechanism and sensor suite. In the work reported here, a lateral pulse jet control mechanism is considered. The lateral pulse jet mechanism consists of a finite number of small thrusters spaced equally around the circumference of the rocket. Using a simulation model that includes projectile, flight control system, and inertial measurement unit dynamics, three different control laws are contrasted, namely, proportional navigation guidance, parabolic and proportional navigation guidance, and trajectory tracking control laws. When the number of individual pulse jets is small, a trajectory tracking control law provides superior dispersion reduction. However, as the number of pulse jets is increased, the relative performance of the parabolic and proportional navigation guidance control law is slightly better than the trajectory tracking control law. When the number of pulse jets is small, the proportional navigation guidance, as well as the parabolic and proportional navigation guidance control laws, exhibits large mean miss distance. All control laws appear to be equally susceptible to accelerometer and gyroscope errors that corrupt inertial measurement unit rocket state feedback.

Contents

List of Figures	v
1. Introduction	1
2. Simulation Model	2
2.1 Flight Control Laws.....	2
2.1.1 PNG.....	3
2.1.2 PAPNG.....	5
2.1.3 TT.....	6
2.2 Lateral Pulse Jet Firing Logic	6
3. Results	7
4. Conclusions	9
5. References	21
Distribution List	23
Report Documentation Page	29

INTENTIONALLY LEFT BLANK.

List of Figures

Figure 1. Schematic of a direct fire rocket with a lateral pulse jet.....	11
Figure 2. LOS reference frame schematic.	11
Figure 3. PNG control law in the horizontal plane.....	12
Figure 4. Parabolic trajectory in the LOS reference frame.....	12
Figure 5. Parabolic navigation guidance control law in the vertical plane.	13
Figure 6. TT control law.....	13
Figure 7. The i^{th} individual lateral pulse jet firing logic.....	14
Figure 8. Altitude vs. range.	15
Figure 9. Cross range vs. range.....	15
Figure 10. Comparison of dispersion radius for pulse jet impulse = 1 N-s.....	16
Figure 11. Comparison of mean miss distance for pulse jet impulse = 1 N-s.	16
Figure 12. Comparison of dispersion radius for pulse jet impulse = 5 N-s.....	17
Figure 13. Comparison of mean miss distance for pulse jet impulse = 5 N-s.	17
Figure 14. Comparison of dispersion radius for pulse jet impulse = 10 N-s.....	18
Figure 15. Comparison of mean miss distance for pulse jet impulse = 10 N-s.....	18
Figure 16. Effect of accelerometer bias on dispersion radius.	19
Figure 17. Effect of accelerometer bias on mean miss distance.....	19
Figure 18. Effect of gyroscope bias on dispersion radius.	20
Figure 19. Effect of gyroscope bias on mean miss distance.....	20

INTENTIONALLY LEFT BLANK.

1. Introduction

Direct fire atmospheric rockets are commonly used munitions on the battlefield and are launched from both land and air delivery platforms. The popularity of these weapons stems from the low system weight and relatively low unit cost. Compared to gun-launched projectiles, uncontrolled direct fire rockets are very inaccurate and are viewed as area weapons on the battlefield. Poor accuracy characteristics of direct fire rockets stems from the fact that the rocket enters the atmosphere with low speed. Any atmospheric or motion disturbances experienced by the rocket at launch map into comparatively large aerodynamic angles of attack causing aerodynamic jump that leads to high impact point dispersion.

In order to improve impact point accuracy performance, weapon system developers are now considering the use of active flight control. A possible control mechanism to suit this purpose is a lateral pulse jet control mechanism. The lateral pulse jet mechanism consists of a ring of small thrusters mounted near the nose of the rocket. Each thruster on the ring imparts a single, short duration, large lateral force to the rocket. Design of a lateral pulse jet flight control system simplifies determining the firing time for each thruster. The lateral pulse jet control mechanism falls into the category of an impulse control mechanism. This is in contrast to the vast majority of flight control mechanisms, such as deflecting fins that continuously generate a control force to track a specific trajectory. While highly developed techniques such as proportional navigation guidance (PNG) are well known in missile guidance where continuous control is available, few have focused attention on the use of impulse control mechanisms, particularly for direct fire rockets. Harkins and Brown [1] developed a simple control scheme to reduce dispersion of a direct fire rocket which only required angular rate feedback. For the example configuration considered, impact point dispersion was reduced by a factor of 4. Jitraphai and Costello [2] studied the same problem using a trajectory tracking flight control law which required an inertial measurement unit (IMU). Rocket dispersion was reduced by as much as a factor of 100, depending on the lateral pulse jet configuration. Calise and El-Shirbiny [3] developed a lateral pulse jet control law for a spin-stabilized gun-launched projectile based on proportional navigation guidance, but modified to account for trajectory bending due to gravity.

The work reported here uses dynamic simulation to compare the merits of different flight control laws specifically applied to a direct fire atmospheric rocket equipped with a lateral pulse jet control mechanism. Candidate flight control laws include: PNG, parabolic and proportional navigation guidance (PAPNG), and trajectory tracking (TT). Parametric studies considering the effect

of the number of individual pulse jets, the impulse of each thruster, and sensor errors on dispersion, and mean miss distance are reported.

2. Simulation Model

The system under consideration is an atmospheric rocket equipped with a flight control system. The control mechanism system is a ring of lateral pulse jets, an IMU, and associated electronics. The coupled dynamics of the rocket, IMU, and flight control law are included in the simulation model deployed in this study. A schematic of the overall system is shown in Figure 1.

As is typical in flight dynamic modeling of projectiles, the rocket is modeled as a rigid body described by six degrees of freedom (6-DOF). The 6-DOF are the three position components of the mass center and the three Euler orientation angles. Forces and moments acting on the body include weight, air loads, main rocket motor thrust, and lateral pulse jet thrust. Details on the dynamic model of the rocket are available elsewhere and are omitted here for brevity [2, 4]. Sensor feedback used by the flight control law is obtained with a conventional IMU. The IMU contains three translational accelerometers and three rate gyroscopes that provide the acceleration of the IMU location and the angular velocity of the rocket with respect to the ground expressed in the rocket reference frame. The IMU estimates the position, orientation, and velocity of the rocket by numerically integrating kinematic and dynamic equations. Merhav [5] provides details on conventional IMU dynamic equations. Accuracy of the IMU is largely dependent on two factors, namely, accuracy of the initial position, orientation, and velocity used by the IMU as it begins to integrate the dynamics equations and errors in the accelerometers and gyroscopes. In order to model the effect of sensor errors in the dynamics of the IMU, filtered Gaussian random noise and bias is added to each of the sensors.

Simulation of the controlled rocket system entails numerically integrating 21 nonlinear ordinary differential equations, 12 equations for the rocket, and 9 equations for the IMU. These equations are integrated forward in time using an adaptive time step Runge-Kutta method [6].

2.1 Flight Control Laws

Three different control laws are considered for a direct fire atmospheric rocket with a lateral pulse jet control mechanism. The control laws consist of control logic to generate an appropriate error signal and control logic to fire the lateral pulse jets. The lateral pulse jet firing logic is the same for all three flight control laws and is described at the end of this section.

2.1.1 PNG

Developed during World War II, PNG is a well-known guidance technique for tactical and strategic missiles and will act as a benchmark control law. PNG issues command accelerations calculated during flight that are proportional to the line-of-sight (LOS) angular rate, \dot{I} , and the rocket closing velocity, V_C . Mathematically, the guidance law can be stated as shown in equation (1):

$$A_C = NV_C \dot{I} \quad (1)$$

In equation (1), N is the proportional navigation constant that is typically set between 3 and 5 [7].

The horizontal plane PNG control law is derived by considering Figure 2. Point P represents a moving projectile that is fired from a launcher towards a target at point T . The LOS frame ($\bar{I}_L, \bar{J}_L, \bar{K}_L$) is defined with its origin at point P . The \bar{I}_L unit vector lies on the horizontal plane projection of the line between the projectile and the target. The \bar{J}_L unit vector lies on the horizontal plane and the \bar{K}_L points down. The relationship between the inertial reference frame and the LOS frame is given by a rotation matrix defined by equation (2):

$$\begin{Bmatrix} \bar{I}_I \\ \bar{J}_I \\ \bar{K}_I \end{Bmatrix} = \begin{bmatrix} c_{I_H} & -s_{I_H} & 0 \\ s_{I_H} & c_{I_H} & 0 \\ 0 & 0 & 1 \end{bmatrix} \begin{Bmatrix} \bar{I}_L \\ \bar{J}_L \\ \bar{K}_L \end{Bmatrix} = [T_{LI}] \begin{Bmatrix} \bar{I}_L \\ \bar{J}_L \\ \bar{K}_L \end{Bmatrix}, \quad (2)$$

where I_H and \dot{I}_H are determined by equations (3) and (4):

$$I_H = \tan^{-1} \left(\frac{y_T - y}{x_T - x} \right) \quad (3)$$

and

$$\dot{I}_H = \frac{-\dot{y}(x_T - x) + \dot{x}(y_T - y)}{(x_T - x)^2 + (y_T - y)^2}. \quad (4)$$

Equation (4) has been simplified with the assumption that the target is stationary. The horizontal acceleration command is given by equation (5):

$$\tilde{A}_{YC} = N_H \dot{I}_H u_H \quad (5)$$

$$u_H = c_{I_H} \dot{x} + s_{I_H} \dot{y} \quad (6)$$

Figure 3 shows the flight control system block diagram of the horizontal guidance law.

The vertical plane PNG control law can be derived in the same manner. The final vertical plane guidance commands are given by equations (7)–(10):

$$\mathbf{I}_V = \tan^{-1} \left(\frac{z_T - z}{x_T - x} \right), \quad (7)$$

$$\dot{\mathbf{I}}_V = \frac{-\dot{z}(x_T - x) + \dot{x}(z_T - z)}{(x_T - x)^2 + (z_T - z)^2}, \quad (8)$$

$$\tilde{A}_{ZC} = N_V \dot{\mathbf{I}}_V u_V, \quad (9)$$

$$u_V = c_{I_V} \dot{x} + s_{I_V} \dot{z}. \quad (10)$$

Equation (8) has been simplified with the assumption that the target is stationary. The vertical acceleration command magnitude is given by equation (9).

The total acceleration command in the LOS frame is given by equation (11):

$$\tilde{\mathbf{A}}_C = \tilde{A}_{YC} \tilde{\mathbf{J}}_L + \tilde{A}_{ZC} \tilde{\mathbf{K}}_L = A_{XC} \tilde{\mathbf{I}}_B + A_{YC} \tilde{\mathbf{J}}_B + A_{ZC} \tilde{\mathbf{K}}_B. \quad (11)$$

The command acceleration components are transformed to the projectile body frame by first transforming the command acceleration components from the LOS frame to the inertial frame and then to the body frame. Equation (12) provides the transfer formula:

$$\begin{Bmatrix} A_{XC} \\ A_{YC} \\ A_{ZC} \end{Bmatrix} = [T_{IB}] [T_{LI}] \begin{Bmatrix} 0 \\ \tilde{A}_{YC} \\ \tilde{A}_{ZC} \end{Bmatrix}. \quad (12)$$

Note that the tilde symbol (~) indicates that a quantity is described in the LOS reference frame. In equation (12), T_{IB} is the inertial to body reference frame transformation:

$$T_{IB} = \begin{bmatrix} c_q c_y & c_q s_y & -s_q \\ s_f s_q c_y - c_f s_y & s_f s_q s_y + c_f c_y & s_f c_q \\ c_f s_q c_y + s_f s_y & c_f s_q s_y - s_f c_y & c_f c_q \end{bmatrix}. \quad (13)$$

The magnitude of the off-axis command acceleration is used as the error signal that is input to the lateral pulse jet firing logic. Equation (15) provides the error signal phase angle:

$$\Gamma = \sqrt{A_{YC}^2 + A_{ZC}^2}, \quad (14)$$

$$\mathbf{g} = \tan^{-1} \left(\frac{A_{zC}}{A_{yC}} \right). \quad (15)$$

2.1.2 PAPNG

The PAPNG control law uses the same horizontal plane acceleration command as PNG. Thus, \tilde{A}_{yC} is given by equation (5). In the vertical plane, a parabolic guidance law is employed to determine command acceleration in the vertical LOS plane to compensate for trajectory bending due to rocket weight. A desired parabolic trajectory is continuously updated during flight. Figure 4 shows the desired parabolic trajectory described by equation (16) [3].

$$\hat{z}_p = \hat{z}_T + K_1 \hat{x}_p + K_2 \hat{x}_p^2, \quad (16)$$

where \hat{x}_p and \hat{z}_p are components of the projectile position in the target reference frame, and \hat{x}_T and \hat{z}_T are components of the target position in the target reference frame. The target reference frame unit vectors, \bar{I}_T, \bar{J}_T and \bar{K}_T are shown in Figure 4. The \bar{K}_T axis points toward the target point. The vectors \bar{I}_T and \bar{K}_T are parallel but in opposite directions to \bar{I}_L and \bar{K}_L . The parameters K_1 and K_2 are constants determined such that a parabolic trajectory that emanates from the projectile passes through the target and has a specific trajectory angle, \mathbf{b}_F , at the target point.

$$K_1 = \tan(\mathbf{b}_F). \quad (17)$$

$$K_2 = \frac{-(K_1 \sqrt{(x_T - x)^2 + (y_T - y)^2} + \hat{z}_T - \hat{z}_p)}{(x_T - x)^2 + (y_T - y)^2}. \quad (18)$$

The command acceleration component in the vertical LOS plane is determined by equation (19):

$$\tilde{A}_{zC} = \frac{V_L (\mathbf{b}_D - \mathbf{b})}{t}. \quad (19)$$

Figure 5 shows the diagram of the vertical guidance law. In equation (19), V_L is the magnitude of projectile velocity in the LOS frame, \mathbf{b} is the flight path angle of the projectile in the LOS frame, and t is the acceleration command time constant. \mathbf{b}_D is the desired flight path angle of the projectile, which is computed using the parabolic trajectory as shown in Figure 5. The acceleration command in the LOS frame is given in equation (20). It is transformed to the body reference frame using sequences of rotations shown in equation (22).

$$\bar{A}_C = -\tilde{A}_{ZC} s_b \bar{I}_L + \tilde{A}_{YC} \bar{J}_L - \tilde{A}_{ZC} c_b \bar{K}_L . \quad (20)$$

$$\bar{A}_C = A_{XC} \bar{I}_B + A_{YC} \bar{J}_B + A_{ZC} \bar{K}_B . \quad (21)$$

$$\begin{Bmatrix} A_{XC} \\ A_{YC} \\ A_{ZC} \end{Bmatrix} = [T_{IB}] [T_{LI}] \begin{Bmatrix} -s_b \tilde{A}_{ZC} \\ \tilde{A}_{YC} \\ -c_b \tilde{A}_{ZC} \end{Bmatrix} . \quad (22)$$

Using equation (22), the error magnitude and phase of the off-axis command acceleration is computed using equations (14) and (15).

2.1.3 TT

A predetermined command trajectory is assumed to be known prior the launch of the rocket. This command trajectory is a desired path of the rocket from the launcher to the target. For direct fire rockets, a command ballistic trajectory is available from the fire control system and can be downloaded to the rocket just prior to launch. A schematic of the flight control system block diagram is shown in Figure 6.

The TT flight control system first compares the measured position of the projectile (x, y, z) to the commanded trajectory (x_c, y_c, z_c) to form a position error vector in the inertial frame. The trajectory error is converted to the rocket body frame using equation (23):

$$\begin{Bmatrix} e_x \\ e_y \\ e_z \end{Bmatrix} = [T_{IB}] \begin{Bmatrix} x_c - x \\ y_c - y \\ z_c - z \end{Bmatrix} . \quad (23)$$

The magnitude and phase angle of the error in the off-axis plane of the rocket are denoted Γ and g , and are defined by equations (24) and (25), respectively. The error magnitude is used in the firing decision and the error phase angle is used in the selection of pulse jet to be fired:

$$\Gamma = \sqrt{e_y^2 + e_z^2} , \quad (24)$$

$$g = \tan^{-1}(e_z / e_y) . \quad (25)$$

2.2 Lateral Pulse Jet Firing Logic

A schematic diagram of the lateral pulse jet firing logic is given in Figure 7. The same logic is used for all the control laws previously described. At each computation cycle in the flight control system, a sequence of checks are

conducted that govern firing of individual lateral pulse jets. The conditions that must be satisfied for an individual lateral pulse jet to fire are as follows:

- The error magnitude must be greater than a specified tolerance, namely e_{THRES} :

$$\Gamma > e_{THRES} . \quad (26)$$

- The time elapsed since the last lateral pulse jet firing must be greater than a specified duration, Δt_{THRES} . This condition implies a specified delay time between two consecutive firings,

$$t - t^* > \Delta t_{THRES} , \quad (27)$$

where t^* is the time of the most recent pulse jet firing.

- The difference between the error phase angle and the individual pulse jet force must be less than a specified angle, d_{THRES} :

$$\left| \mathbf{f}_{Ji} - \mathbf{p} - \mathbf{g} - \dot{\mathbf{g}} \frac{\Delta_{PJ}}{2} \right| < d_{THRES} . \quad (28)$$

- The individual pulse jet under consideration has not been fired.

The first two checks are valid for all lateral pulse jets while the last two checks are specific to a given lateral pulse jet.

3. Results

The rocket configuration used in the simulation study is a representative direct fire rocket that is a 1.4-m-long, fin-stabilized rocket with three pop-out fins on the rear of the projectile. The lateral pulse jet ring is located 1.2 m from the base of the rocket. The main rocket motor burns for 1.1 s and imparts an impulse to the rocket of 6200 N-s. During the main rocket motor burn, the forward velocity of the rocket is increased from 44 m/s to 770 m/s. The rocket weight, mass center location from the base of the rocket, roll inertia, and pitch inertia before and after burn is 10.4/7.2 kg, 0.85/0.86 m, 0.0077 kg/0.0058 m², and 1.83 kg/1.61 m², respectively. Nominally, the rocket exits the launcher with the following initial conditions: $x = 0.0$ m, $y = 0.0$ m, $z = -30.5$ m, $f = 0.0^\circ$, $q = 4.14^\circ$, $\gamma = 0.0^\circ$, $u = 43.7$ m/s, $v = 0.0$ m/s, $w = 0.11$ m/s, $p = 51.5$ rad/s, $q = 0.18$ rad/s, and $r = 0.0$ rad/s.

Using the control laws previously described, uncontrolled and controlled trajectories are compared for the example rocket configuration against a nominal command trajectory. The rocket is launched at an altitude of 30.5 m toward a

target on the ground with altitude and cross range equal zero at a range of 3000 m. The ring contains 32 individual lateral pulse jets where each individual pulse jet imparts an impulse of 5 N-s on the projectile body over a time duration of 0.01 s. The pulse jet elapsed time threshold is set to 0.2 s. The pulse jet angle threshold is set to 0.2°. For the controlled rocket with TT flight control system the window size is 1.5 m. The controlled rocket with PNG or PAPNG flight control system has a window size setting of 6 m/s². These window sizes were optimized through parametric studies in which dispersion was minimized.

Figures 8 and 9 compare the trajectory response obtained using the different guidance schemes. These two figures show a desired controlled trajectory, an uncontrolled trajectory, a PNG controlled trajectory, a PAPNG controlled trajectory, and a TT controlled trajectory. Without the use of pulse jet control, the rocket falls short of the target with a miss distance of 52.5 m. The PAPNG and TT control laws significantly reduce miss distance from 52.5 m in the uncontrolled case to 1.6 and 0.7 m in the controlled case, respectively. Note that the PNG control law actually increases miss distance relative to the uncontrolled case. This is due to the fact that the PNG control law initially commands a downward vehicle acceleration when in fact an upward command acceleration is required to reduce miss distance. Toward the end of the trajectory, the lateral pulse jets do not process sufficient control power to maneuver to the target.

If several projectiles are fired from the same weapon with the same firing setting, their points of impact will be different due to system uncertainty. For direct fire rockets, impact points are defined as the altitude and cross range of the projectile at a specified down range distance. The mean impact point of a group of fired rockets with respect to the target center is a measure of the accuracy of the weapon. The degree of scatter of the impact points about the mean impact point defines dispersion. Both accuracy and dispersion determine whether a particular weapon can hit an intended target.

Scatter in projectile impact points is caused by a myriad of weapon system inaccuracies including launcher manufacturing tolerances, launcher vibration, propellant ignition variation, temperature variations of the launcher or projectile, atmospheric turbulence and gusts, atmospheric pressure variation, etc. For weapon system variations connected with the launch dynamics, the end result is a variation in the initial launch conditions for each projectile fired. Notable launch conditions that create significant impact point scatter are the initial angular velocity of the projectile. To simulate launch conditions that cause dispersion, the initial pitch and yaw rate are modeled as independent Gaussian random variables with a mean and standard deviation of -0.18/0.3 and 0/0.3 rad/s, respectively. The dispersion radius is defined as the radius of a circle that emanates from the mean impact point and contains 67% of the impact points.

Figures 10–15 compare the dispersion radius and mean impact point at a range of 3000 m for PNG, PAPNG, and TT control laws using different combinations of pulse jets. The dispersion radius and mean impact point statistics are computed with a sample size of 200.

Figures 10 and 11 consider 1 N-s pulses, while Figures 12 and 13 consider 5 N-s pulses, and Figures 14 and 15 consider 10 N-s pulses. In all cases, dispersion radius is steadily reduced as the number of pulses is increased. For a relatively small number of pulses, the TT control law provides the lowest dispersion. However, as the number of pulses is increased, the PAPNG control law improves relative to the TT control law and obtains slightly lowest dispersion for a large number of pulse jets. For the PNG and PAPNG control laws, the mean miss distance initially increases as the number of pulse jets is increased and then is reduced as the number of pulse jets continues to increase. For a small number of pulse jets, the mean miss distance is greater than the uncontrolled case. During the thrusting phase of flight, the PNG and PAPNG control laws tend to overcompensate by pulsing too often and are unable to close on the target. The TT control law steadily reduces the mean miss distance as the number of pulse jets is increased.

Figures 16 and 17 examine the sensitivity of the different pulse jet control laws to accelerometer bias errors for the case of 24 individual pulse jets, each with an impulse of 10 Ns. The bias errors for each accelerometer in the IMU are independent Gaussian random variables with zero mean. A sample size of 200 is used to compute the statistics shown in these figures. As the standard deviation of accelerometer bias is increased, dispersion is steadily increased for all control laws. The slope of dispersion radius vs. standard deviation of accelerometer bias error is slightly larger for the TT control law, indicating a larger sensitivity to accelerometer bias errors. The mean miss distance increases as the standard deviation of accelerometer bias error increases for the PNG control law and is flat for the PNG and TT control laws. Figures 18 and 19 are similar to Figures 16 and 17 except gyroscope bias errors in the IMU are evaluated. The slope of dispersion radius vs. gyroscope bias error is lowest for the TT control law indicating the TT control law is comparatively less sensitive to gyroscope bias error. The mean miss distance steadily increases as a function of gyroscope bias error for all control laws.

4. Conclusions

With proper selection of flight control system parameters and adequately sized lateral pulse jets, dispersion and accuracy characteristics of a direct fire rocket equipped with a ring of lateral pulse jets can be drastically improved with a

proportional navigation guidance, proportional and parabolic navigation guidance, or trajectory tracking control law. The proportional navigation guidance control law provided the least dispersion reduction and also generates the largest mean miss distance. This is mainly from target patterns below the target due to gravity effects not accounted for the control law. The proportional and parabolic guidance control law obtained low dispersion and mean miss distance performance when the number of pulse jets is large. The proportional and parabolic guidance control law is comparatively more sensitive to gyroscope bias errors than accelerometer bias errors. The TT control law generated low dispersion and miss distance characteristics, particularly when the number of pulse jets is relatively small. While the proportional navigation guidance control law and the proportional and parabolic navigation guidance control law generated impact patterns off target when the number of pulse jets was low, the TT control law consistently generated impact patterns nearly centered on the target. This is due to the fact that the TT control law forms an error signal from position, whereas the other two control laws use acceleration as the basis for an error signal.

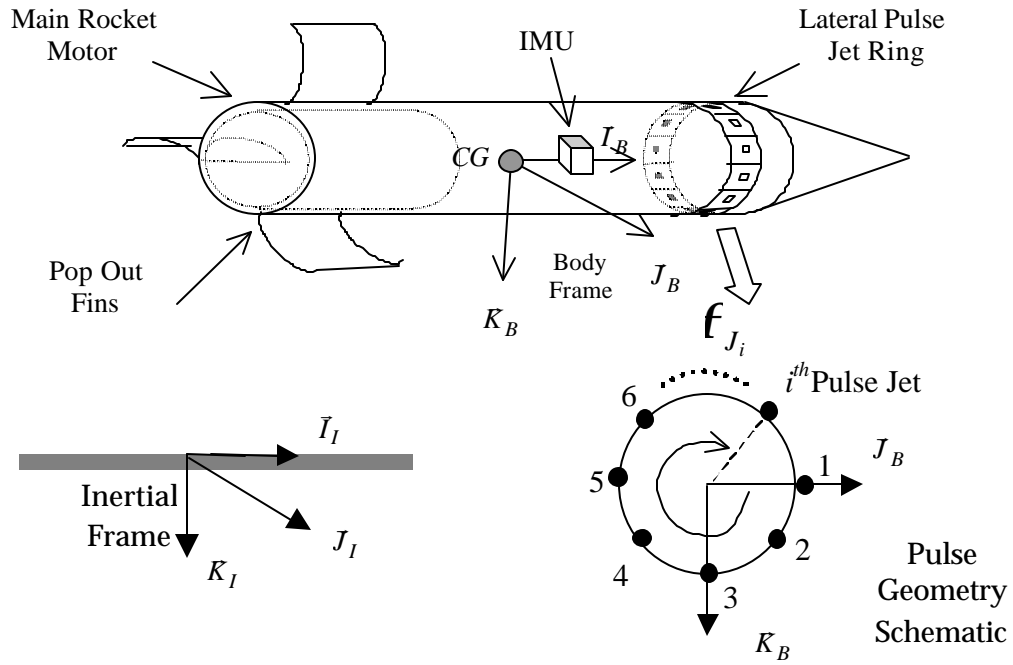


Figure 1. Schematic of a direct fire rocket with a lateral pulse jet.

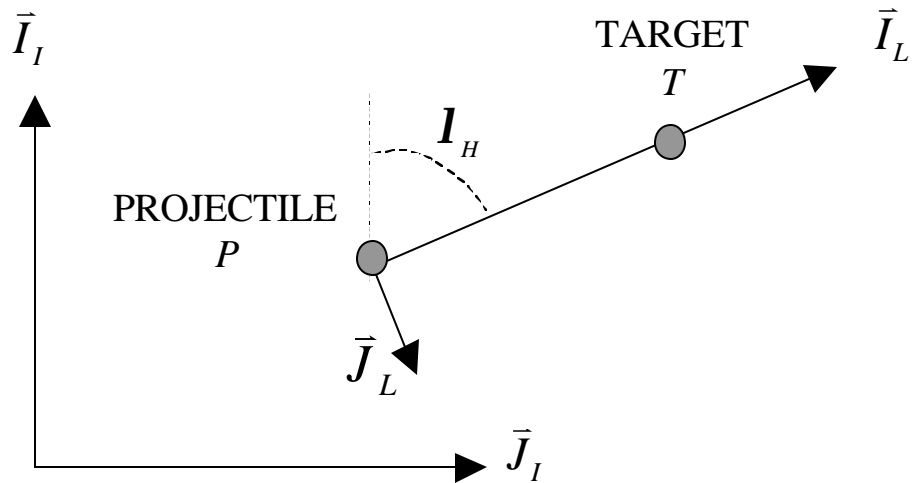


Figure 2. LOS reference frame schematic.

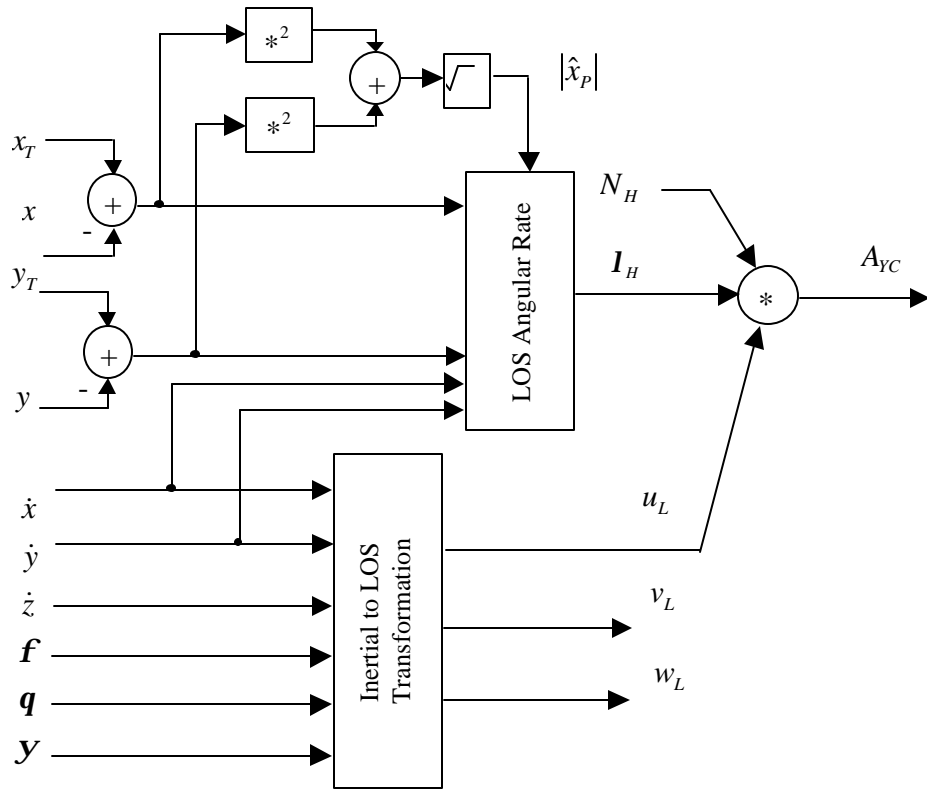


Figure 3. PNG control law in the horizontal plane.

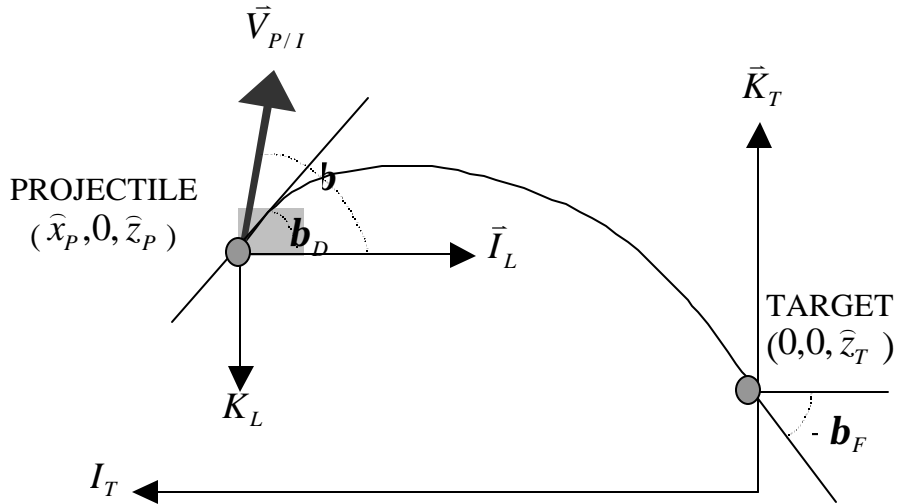


Figure 4. Parabolic trajectory in the LOS reference frame.

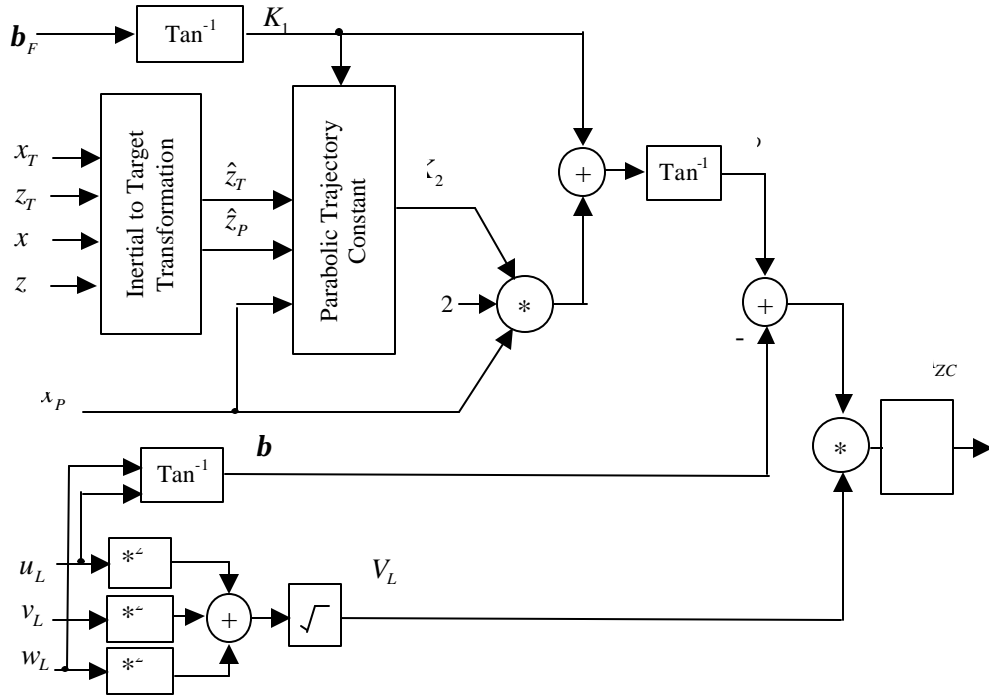


Figure 5. Parabolic navigation guidance control law in the vertical plane.

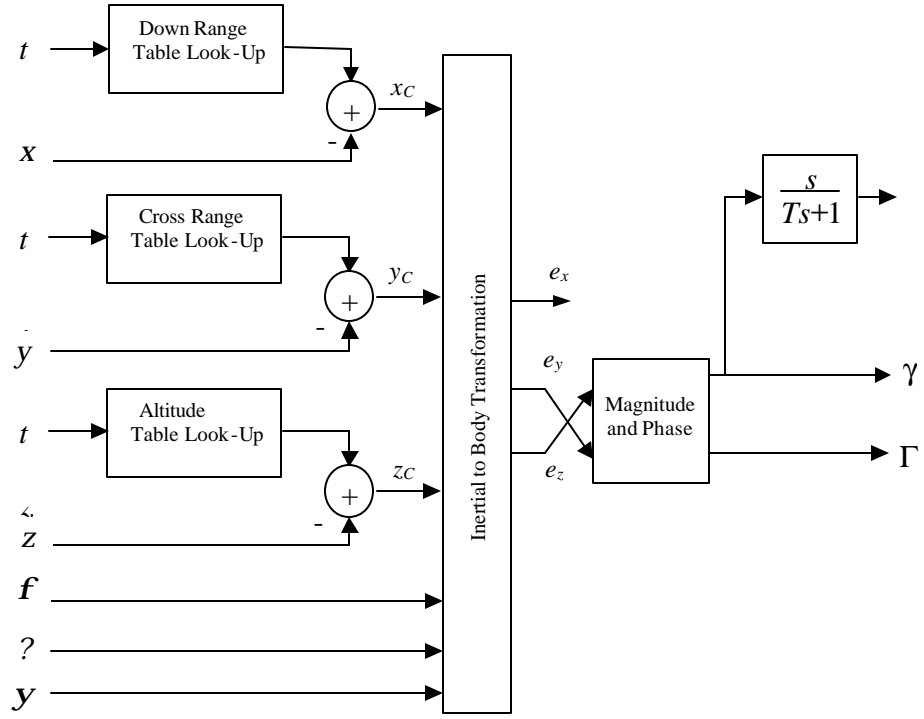


Figure 6. TT control law.

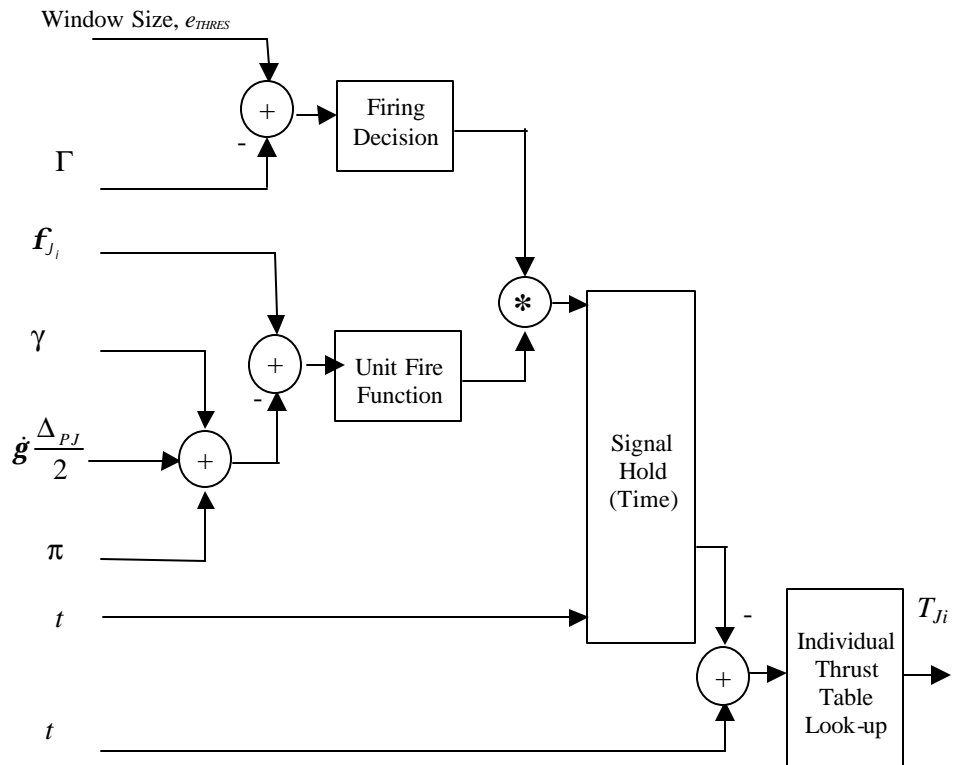


Figure 7. The i^{th} individual lateral pulse jet firing logic.

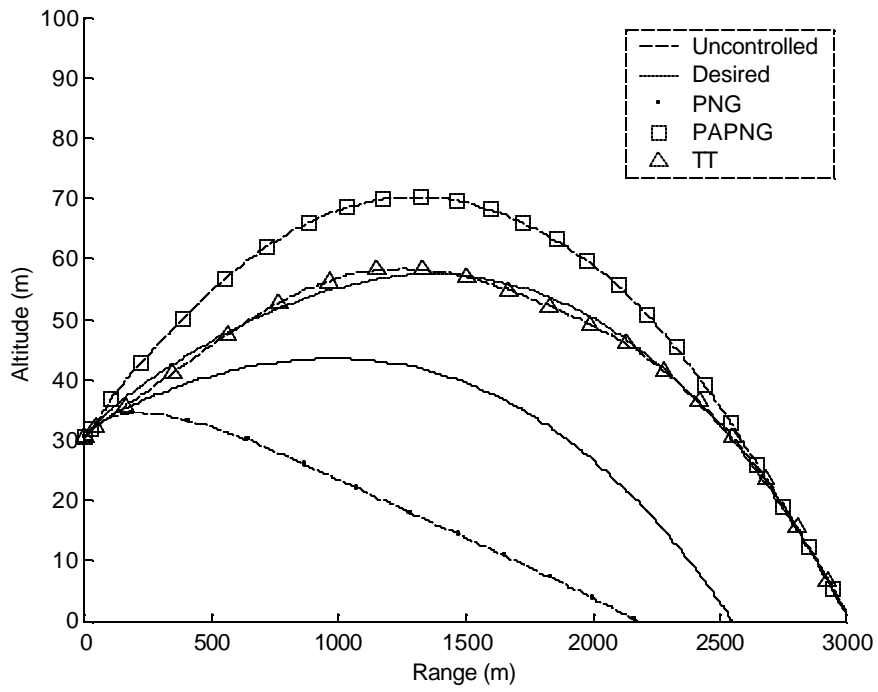


Figure 8. Altitude vs. range.

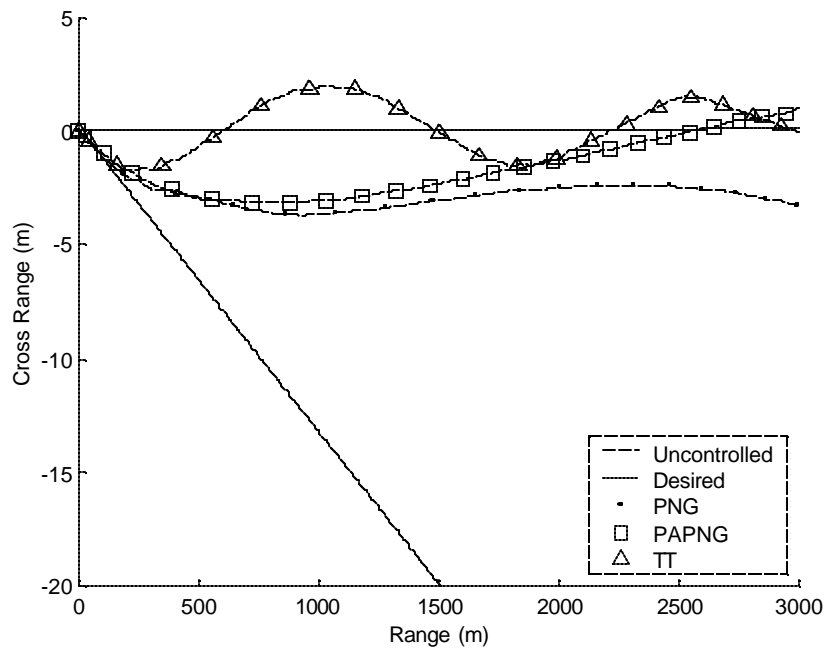


Figure 9. Cross range vs. range.

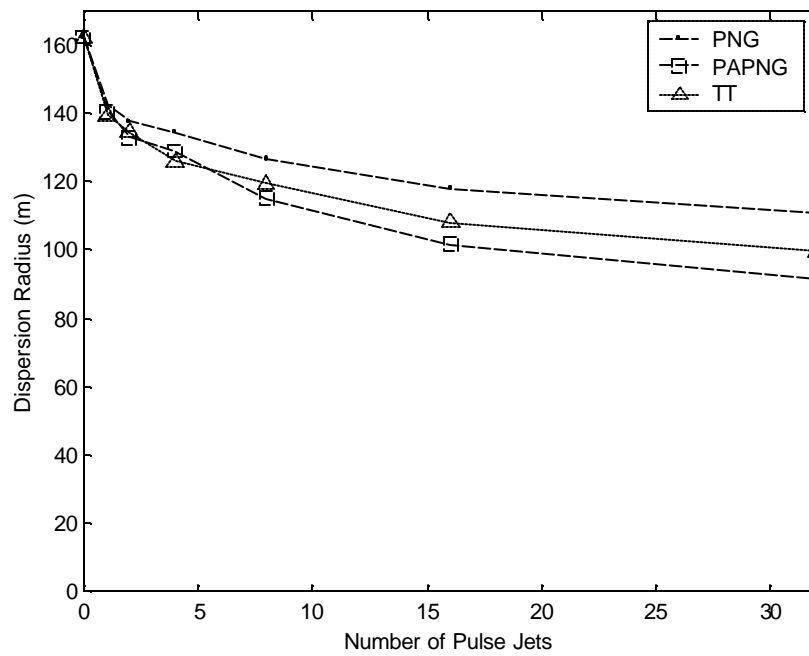


Figure 10. Comparison of dispersion radius for pulse jet impulse = 1 N-s.

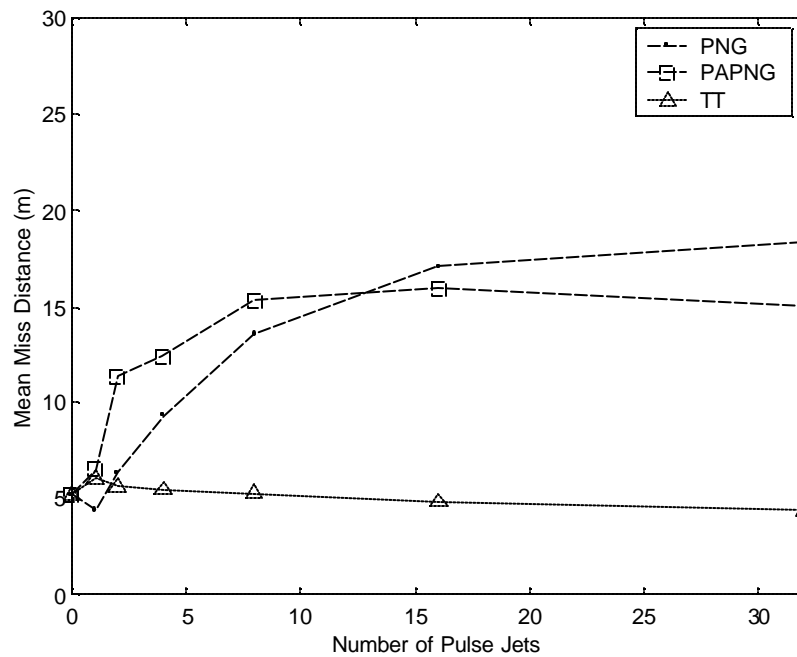


Figure 11. Comparison of mean miss distance for pulse jet impulse = 1 N-s.

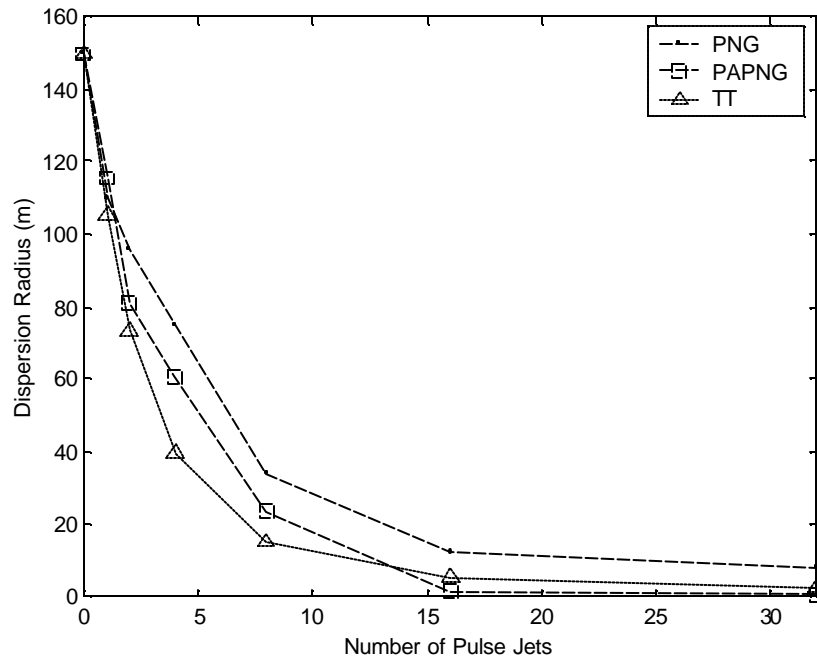


Figure 12. Comparison of dispersion radius for pulse jet impulse = 5 N-s.

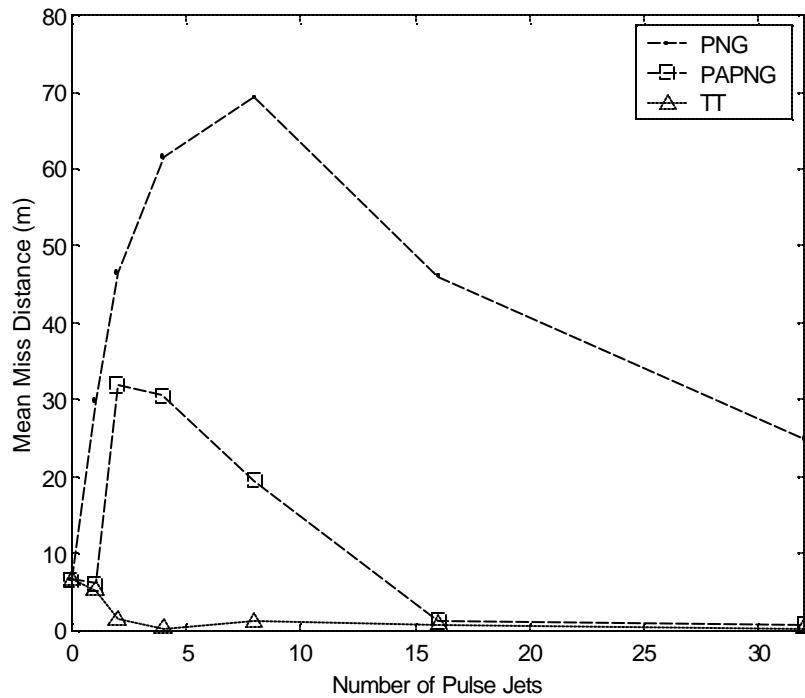


Figure 13. Comparison of mean miss distance for pulse jet impulse = 5 N-s.

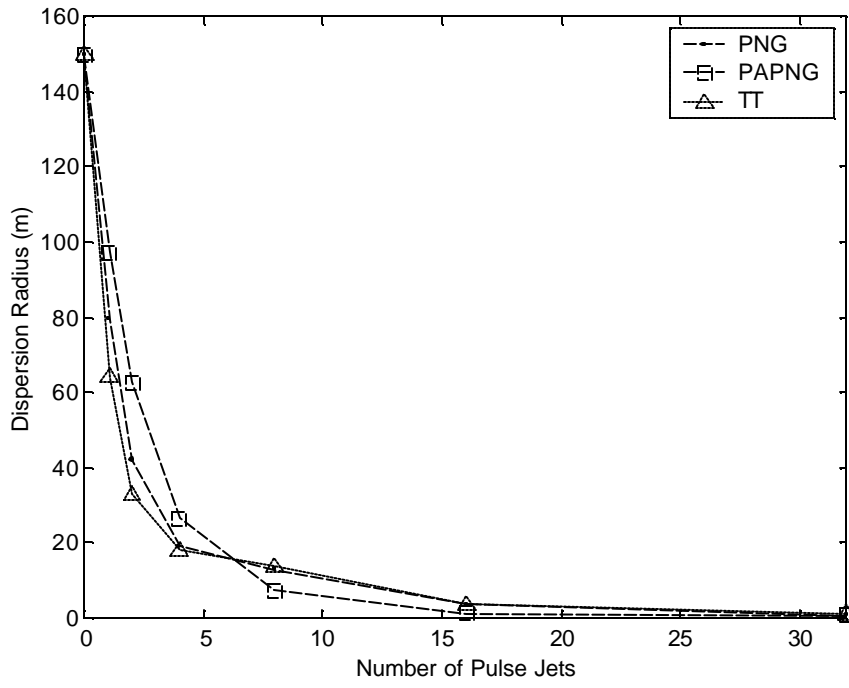


Figure 14. Comparison of dispersion radius for pulse jet impulse = 10 N-s.

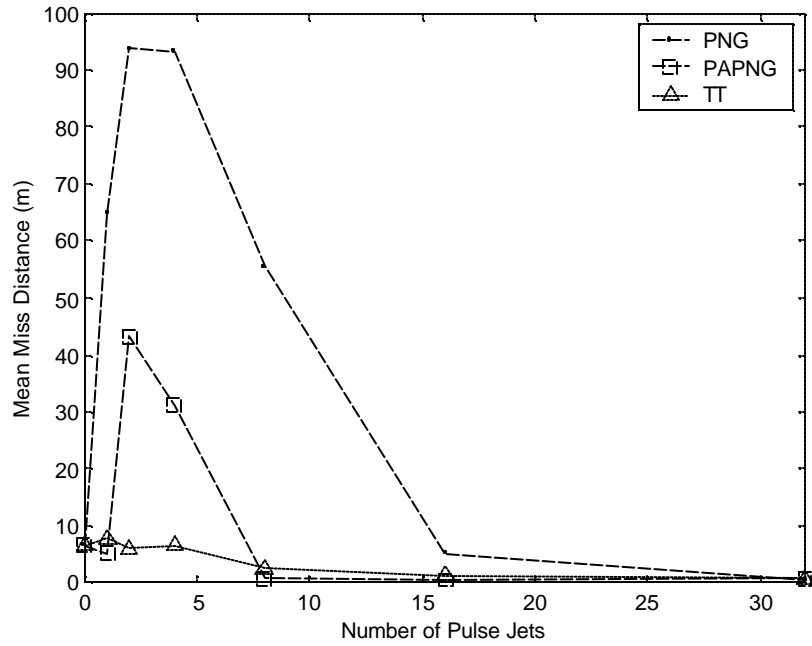


Figure 15. Comparison of mean miss distance for pulse jet impulse = 10 N-s.

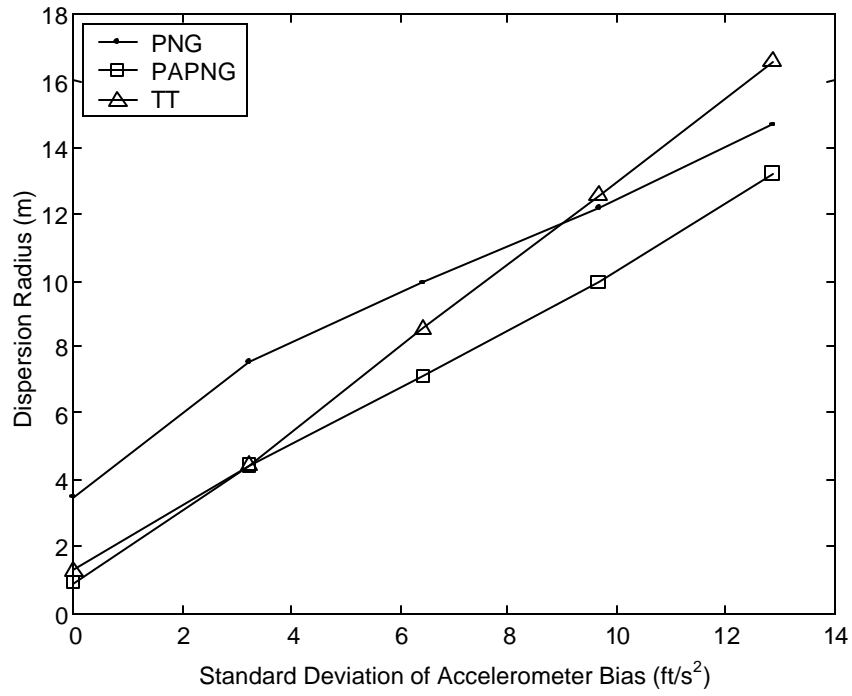


Figure 16. Effect of accelerometer bias on dispersion radius.

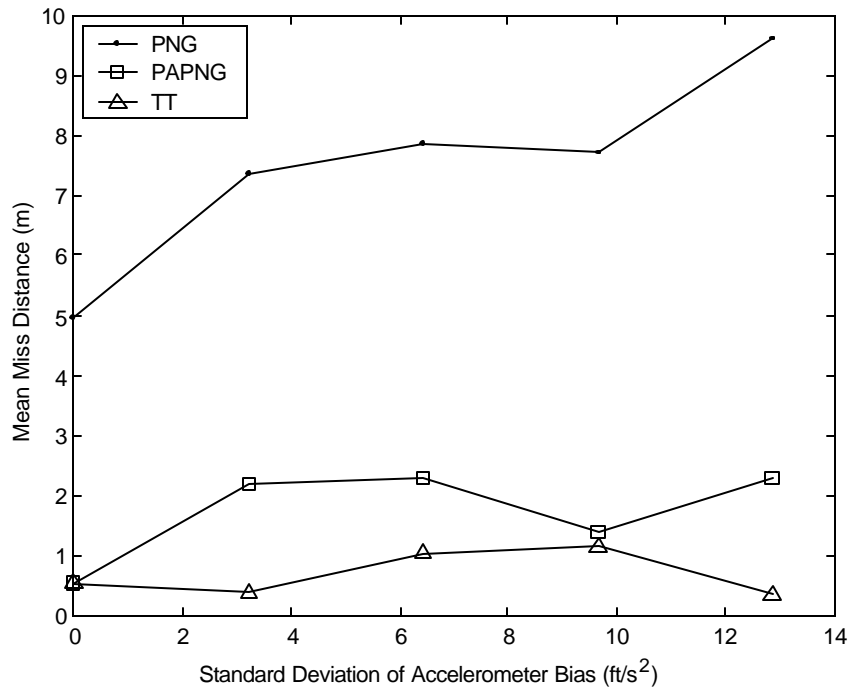


Figure 17. Effect of accelerometer bias on mean miss distance.

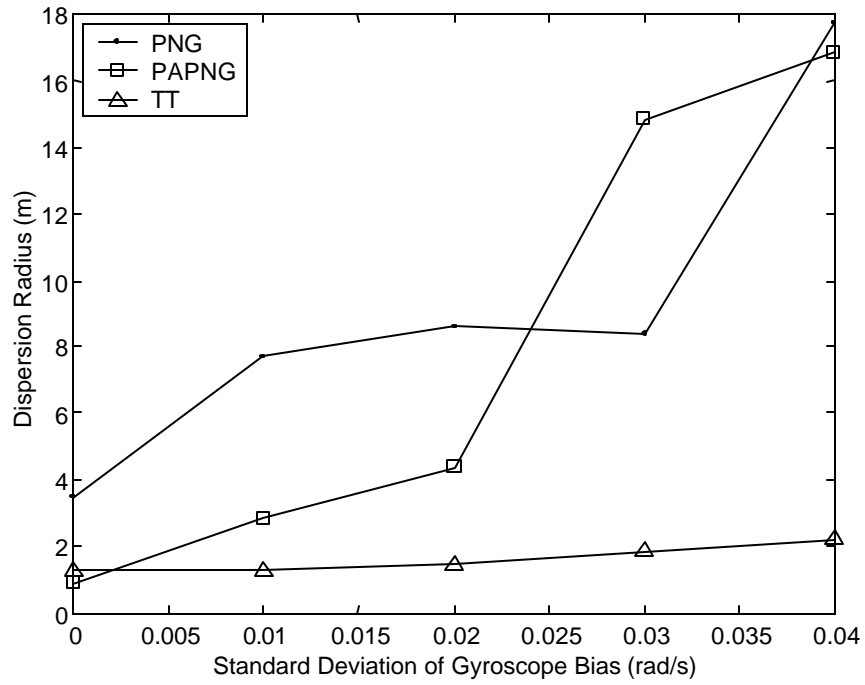


Figure 18. Effect of gyroscope bias on dispersion radius.

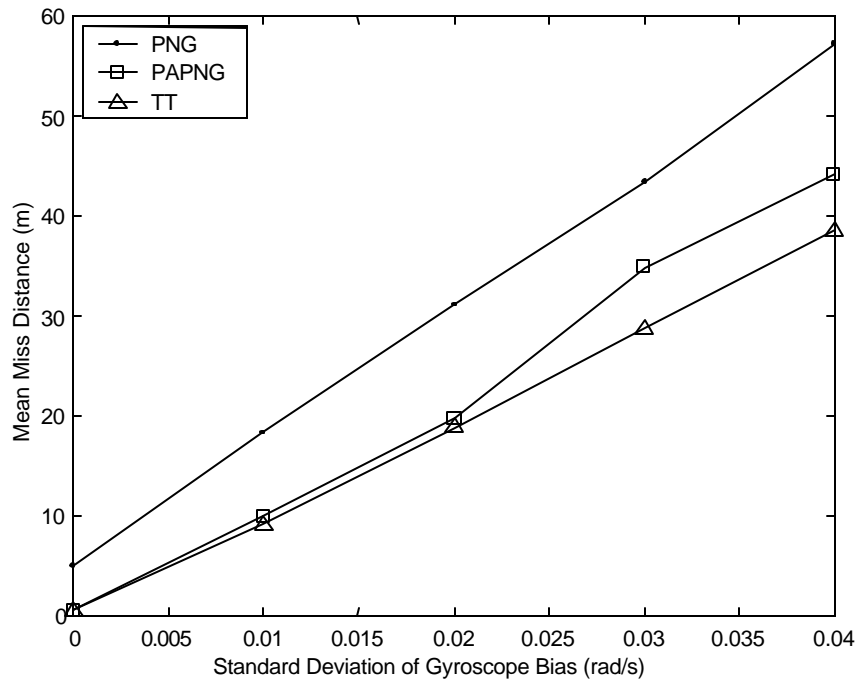


Figure 19. Effect of gyroscope bias on mean miss distance.

5. References

1. Harkins, T., and T. Brown. "Using Active Damping as a Precision-Enhancing Technology for 2.75-inch Rockets." ARL-TR-1772, U.S. Army Research Laboratory, Aberdeen Proving Ground, MD, 1999.
2. Jitraphai, T., and M. Costello. "Dispersion Reduction of a Direct Fire Rocket Using Lateral Pulse Jets." *Journal of Spacecraft and Rocket*, vol. 38, no. 5, 2001.
3. Calise, A., and H. El-Shirbiny. "An Analysis of Aerodynamic Control for Direct Fire Spinning Projectiles." *Proceedings of the 2001 American Institute of Aeronautics and Astronautics Guidance, Navigation, and Control Conference*, AIAA 2001-4217, Montreal, Canada, 2001.
4. Gast, R., S. Morris, and M. Costello. "Simulation of Shot Impacts for the M1A1 Tank Gun." *Journal of Guidance, Control, and Dynamics*, vol. 23, no. 1, pp. 53-59, 2000.
5. Merhav, S. *Aerospace Sensor Systems and Applications*. New York: Springer-Verlag, 1996.
6. Press, W. H., S. A. Teukolsky, W. T. Vetterling, and B. P. Flannery. *Numerical Recipes in Fortran 77: The Art of Scientific Computing, Vol. 1*. Cambridge: Press Syndicate of the University of Cambridge, 1992.
7. Zarchan, P. "Tactical and Strategic Missile Guidance." *Progress in Astronautics and Aeronautics*, vol. 124, pp. 139-180, American Institute of Aeronautics and Astronautics, Inc., Washington, DC, 1990.

INTENTIONALLY LEFT BLANK.

<u>NO. OF COPIES</u>	<u>ORGANIZATION</u>
2	DEFENSE TECHNICAL INFORMATION CENTER DTIC OCA 8725 JOHN J KINGMAN RD STE 0944 FT BELVOIR VA 22060-6218
1	HQDA DAMO FDT 400 ARMY PENTAGON WASHINGTON DC 20310-0460
1	OSD OUSD(A&T)/ODDR&E(R) DR R J TREW 3800 DEFENSE PENTAGON WASHINGTON DC 20301-3800
1	COMMANDING GENERAL US ARMY MATERIEL CMD AMCRDA TF 5001 EISENHOWER AVE ALEXANDRIA VA 22333-0001
1	INST FOR ADVNCD TCHNLGY THE UNIV OF TEXAS AT AUSTIN 3925 W BRAKER LN STE 400 AUSTIN TX 78759-5316
1	US MILITARY ACADEMY MATH SCI CTR EXCELLENCE MADN MATH THAYER HALL WEST POINT NY 10996-1786
1	DIRECTOR US ARMY RESEARCH LAB AMSRL D DR D SMITH 2800 POWDER MILL RD ADELPHI MD 20783-1197
1	DIRECTOR US ARMY RESEARCH LAB AMSRL CI AI R 2800 POWDER MILL RD ADELPHI MD 20783-1197

<u>NO. OF COPIES</u>	<u>ORGANIZATION</u>
3	DIRECTOR US ARMY RESEARCH LAB AMSRL CI LL 2800 POWDER MILL RD ADELPHI MD 20783-1197
3	DIRECTOR US ARMY RESEARCH LAB AMSRL CI IS T 2800 POWDER MILL RD ADELPHI MD 20783-1197
	<u>ABERDEEN PROVING GROUND</u>
2	DIR USARL AMSRL CI LP (BLDG 305)

<u>NO. OF COPIES</u>	<u>ORGANIZATION</u>	<u>NO. OF COPIES</u>	<u>ORGANIZATION</u>
3	AIR FORCE RSRCH LAB MUNITIONS DIR AFRL/MNAV G ABATE 101 W EGLIN BLVD STE 219 EGLIN AFB FL 32542	10	CDR US ARMY TACOM AMCPEO HFM AMCPEO HFM F AMCPEO HFM C AMCPM ABMS AMCPM BLOCKIII AMSTA CF AMSTA Z AMSTA ZD AMCPM ABMS S W DR PATTISON A HAVERILLA WARREN MI 48397-5000
1	CDR WL/MNMF D MABRY 101 W EGLIN BLVD STE 219 EGLIN AFB FL 32542-6810		
20	OREGON STATE UNIVERSITY DEPT OF MECHL ENGRG M COSTELLO CORVALLIS OR 97331	1	CDR USAOTEA CSTE CCA DR RUSSELL ALEXANDRIA VA 22302-1458
4	CDR US ARMY ARDEC AMSTA AR CCH J DELORENZO S MUSALI R SAYER P DONADIO PICATINNY ARESENAL NJ 07806-5000	2	DIR US ARMY ARMOR CTR & SCHL ATSB WP ORSA A POMEY ATSB CDC FT KNOX KY 40121
7	CDR US ARMY TANK MAIN ARMAMENT SYSTEM AMCPM TMA D GUZIEWICZ R DARCEY C KIMKER R JOINSON E KOPOAC T LOUZIERIO C LEVECHIA PICATINNY ARESENAL NJ 07806-5000	1	CDR US ARMY AMCCOM AMSMC ASR A MR CRAWFORD ROCK ISLAND IL 61299-6000
1	CDR USA YUMA PROV GRND STEYT MTW YUMA AZ 85365-9103	2	PROGRAM MANAGER GROUND WEAPONS MCRDAC LTC VARELA CBGT QUANTICO VA 22134-5000
1	DIR BENET LABORATORIES SMCWV QAR T MCCLOSKEY WATERVLIET NY 12189-5000	4	COMMANDER US ARMY TRADOC ATCD T ATCD TT ATTE ZC ATTG Y FT MONROE VA 23651-5000

<u>NO. OF COPIES</u>	<u>ORGANIZATION</u>	<u>NO. OF COPIES</u>	<u>ORGANIZATION</u>
1	NAWC F PICKETT CODE C2774 CLPL BLDG 1031 CHINA LAKE CA 93555	1	OFC OF ASST SECY OF ARMY FOR R&D SARD TR W MORRISON 2115 JEFFERSON DAVIS HWY ARLINGTON VA 22202-3911
1	NAVAL ORDNANCE STATION ADVNC D SYS TCHNLGY BRNCH D HOLMES CODE 2011 LOUISVILLE KY 40214-5001	2	CDR USARDEC AMSTA FSP A S DEFEO R SICIGNANO PICATINNY ARESENAL NJ 07806-5000
1	NAVAL SURFACE WARFARE CTR F G MOORE DAHLGREN DIVISION CODE G04 DAHLGREN VA 22448-5000	2	CDR USARDEC AMSTA AR CCH A M PALATHINGAL R CARR PICATINNY ARESENAL NJ 07806-5000
1	US MILITARY ACADEMY MATH SCI CTR OF EXCELLENCE DEPT OF MATHEMATICAL SCI MDN A MAJ DON ENGEN THAYER HALL WEST POINT NY 10996-1786	5	TACOM ARDEC AMSTA AR FSA K CHIEFA AMSTA AR FS A WARNASCH AMSTA AR FSF W RYBA AMSTA AR FSP S PEARCY J HEDDERICH PICATINNY ARESENAL NJ 07806-5000
3	DIR SNL A HODAPP W OBERKAMPF F BLOTTNER DIVISION 1631 ALBUQUERQUE NM 87185	5	CDR US ARMY MICOM AMSMI RD P JACOBS P RUFFIN AMSMI RD MG GA C LEWIS AMSMI RD MG NC C ROBERTS AMSMI RD ST GD D DAVIS RSA AL 35898-5247
3	ALLIANT TECH SYSTEMS C CANDLAND R BURETTA R BECKER 7225 NORTHLAND DR BROOKLYN PARK MN 55428	3	CDR US ARMY AVN TRP CMD DIRECTORATE FOR ENGRNG AMSATR ESW M MAMOUD M JOHNSON J OBERMARK RSA AL 35898-5247
3	DIR USARL AMSRL SE RM H WALLACE AMSRL SS SM J EIKE A LADAS 2800 POWDER MILL RD ADELPHI MD 20783-1145		

<u>NO. OF COPIES</u>	<u>ORGANIZATION</u>	<u>NO. OF COPIES</u>	<u>ORGANIZATION</u>
1	DIR US ARMY RTTC STERT TE F TD R EPPS BLDG 7855 REDSTONE ARSENAL AL 38598-8052	1	CDR NSWC DAHLGREN DIV CODE 40D J BLANKENSHIP 6703 WEST HWY 98 PANAMA CITY FL 32407-7001
2	STRICOM AMFTI EL D SCHNEIDER R COLANGELO 12350 RESEARCH PKWY ORLANDO FL 32826-3276	1	CDR NSWC J FRAYSEE D HAGEN 17320 DAHLGREN RD DAHLGREN VA 22448-5000
1	CDR OFFICE OF NAVAL RES CODE 333 J GOLDWASSER 800 N QUINCY ST RM 507 ARLINGTON VA 22217-5660	5	CDR NSWC INDIAN HEAD DIV CODE 40D D GARVICK CODE 4110C L FAN CODE 4120 V CARLSON CODE 4140E H LAST CODE 450D T GRIFFIN 101 STRAUSS AVE INDIAN HEAD MD 20640-5000
1	CDR US ARMY RES OFFICE AMXRO RT IP TECH LIB PO BOX 12211 RESEARCH TRIANGLE PARK NJ 27709-2211	1	CDR NSWC INDIAN HEAD DIV LIBRARY CODE 8530 BLDG 299 101 STRAUSS AVE INDIAN HEAD MD 20640
4	CDR US ARMY AVN TRP CMD AVIATION APPLIED TECH DIR AMSATR TI R BARLOW E BERCHER T CONDON B TENNEY FT EUSTIS VA 23604-5577	2	US MILITARY ACADEMY MATH SCI CTR OF EXCELLENCE DEPT OF MATHEMATICAL SCI MDN A MAJ D ENGEN R MARCHAND THAYER HALL WEST POINT NY 10996-1786
3	CDR NAWC WEAPONS DIV CODE 543400D S MEYERS CODE C2744 T MUNSINGER CODE C3904 D SCOFIELD CHINA LAKE CA 93555-6100	3	CDR US ARMY YUMA PG STEYP MT AT A A HOOPER STEYP MT EA YUMA AZ 85365-9110
1	CDR NSWC CRANE DIVISION CODE 4024 J SKOMP 300 HIGHWAY 361 CRANE IN 47522-5000		

<u>NO. OF COPIES</u>	<u>ORGANIZATION</u>	<u>NO. OF COPIES</u>	<u>ORGANIZATION</u>
6	CDR NSWC INDIAN HEAD DIV CODE 570D J BOKSER CODE 5710 L EAGLES J FERSUSON CODE 57 C PARIS CODE 5710G S KIM CODE 5710E S JAGO 101 STRAUSS AVE ELY BLDG INDIAN HEAD MD 20640-5035		<u>ABERDEEN PROVING GROUND</u>
1	B KIM MICHIGAN STATE UNIVERSITY 2120 ENGINEERING BLDG EAST LANSING MI 48824-1226	3	CDR USA ARDEC AMSTA AR FSF T R LIESKE J WHITESIDE J MATTS BLDG 120
2	INDUSTRIAL OPERATION CMD AMFIO PM RO W MCKELVIN MAJ BATEMAN ROCK ISLAND IL 61299-6000	1	CDR USA TECOM AMSTE CT T J SCHNELL RYAN BLDG
3	PROGRAM EXECUTIVE OFFICER TACTICAL AIRCRAFT PROGRAMS PMA 242 1 MAJ KIRBY R242 PMA 242 33 R KEISER (2 CPS) 1421 JEFFERSON DAVIS HWY ARLINGTON VA 22243-1276	3	CDR USA AMSAA AMXSY EV G CASTLEBURY R MIRABELLE AMXSY EF S MCKEY
1	CDR NAVAL AIR SYSTEMS CMD CODE AIR 471 A NAKAS 1421 JEFFERSON DAVIS HWY ARLINGTON VA 22243-1276	47	DIR USARL AMSRL CI HC S WILKERSON AMSRL SL BE A MIKHAIL AMSRL WM B W CIEPIELA A W HORST JR AMSRL WM BA F BRANDON T G BROWN (5 CPS) L BURKE J CONDON B DAVIS T HARKINS (5 CPS) D HEPNER M HOLLIS V LEITZKE D LYON A THOMPSON
3	ARROW TECH ASSOCIATES INC R WHYTE A HATHAWAY H STEINHOFF 1233 SHELBOURNE RD SUITE D8 SOUTH BURLINGTON VT 05403		AMSRL WM BC M BUNDY G COOPER J GARNER B GUIDOS J NEWILL V OSKAY P PLOSTINS (4 CPS)
3	US ARMY AVIATION CTR DIR OF COMBAT DEVELOPMENT ATZQ CDM C B NELSON ATZQ CDC C T HUNDLEY ATZQ CD G HARRISON FORT RUCKER AL 36362		

NO. OF
COPIES ORGANIZATION

ABERDEEN PROVING GROUND (CONTD)

J SAHU
K SOENCKSEN
AMSRL WM BD
B FORCH
AMSRL WM BE
E M SCHMIDT
AMSRL WM BF
B HAUG
P HILL
J LACETERA
J WALL
AMSRL WM MB
J BENDER
W DRYSDALE
AMSRL WM RP
J BORNSTEIN
C SHOEMAKER
AMSRL WM SG
T ROSENBERGER
AMSRL WM TC
R COATES

REPORT DOCUMENTATION PAGE			Form Approved OMB No. 0704-0188	
Public reporting burden for this collection of information is estimated to average 1 hour per response, including the time for reviewing instructions, searching existing data sources, gathering and maintaining the data needed, and completing and reviewing the collection of information. Send comments regarding this burden estimate or any other aspect of this collection of information, including suggestions for reducing this burden, to Washington Headquarters Service, Directorate for Information Operations and Reports, 1215 Jefferson Davis Highway, Suite 1204, Arlington, VA 22202-4302, and to the Office of Management and Budget, Paperwork Reduction Project (0704-0188), Washington, DC 20503.				
1. AGENCY USE ONLY (Leave blank)	2. REPORT DATE April 2002	3. REPORT TYPE AND DATES COVERED Final, September 2001-September 2002		
4. TITLE AND SUBTITLE A Comparison of Different Guidance Schemes for a Direct Fire Rocket With a Pulse Jet Control Mechanism			5. FUNDING NUMBERS C: DAAD17-01-P-1038	
6. AUTHOR(S) Thanat Jitpraphai,* Bradley Burchett,* and Mark Costello*				
7. PERFORMING ORGANIZATION NAME(S) AND ADDRESS(ES) Oregon State University Department of Mechanical Engineering Corvallis, OR 97331			8. PERFORMING ORGANIZATION REPORT NUMBER	
9. SPONSORING/MONITORING AGENCY NAME(S) AND ADDRESS(ES) U.S. Army Research Laboratory ATTN: AMSRL-WM-BC Aberdeen Proving Ground, MD 21005-5066			10. SPONSORING/MONITORING AGENCY REPORT NUMBER ARL-CR-493	
11. SUPPLEMENTARY NOTES				
12a. DISTRIBUTION/AVAILABILITY STATEMENT Approved for public release; distribution is unlimited.			12b. DISTRIBUTION CODE	
13. ABSTRACT (Maximum 200 words) Compared to gun launch ammunition, uncontrolled direct fire atmospheric rockets are terribly inaccurate, to the point where they are used most effectively on the battlefield as area weapons. Dispersion characteristics can be dramatically improved by outfitting the rocket with a suitable control mechanism and sensor suite. In the work reported here, a lateral pulse jet control mechanism is considered. The lateral pulse jet mechanism consists of a finite number of small thrusters spaced equally around the circumference of the rocket. Using a simulation model that includes projectile, flight control system, and inertial measurement unit dynamics, three different control laws are contrasted, namely, proportional navigation guidance, parabolic and proportional navigation guidance, and trajectory tracking control laws. When the number of individual pulse jets is small, a trajectory tracking control law provides superior dispersion reduction. However, as the number of pulse jets is increased, the relative performance of the parabolic and proportional navigation guidance control law is slightly better than the trajectory tracking control law. When the number of pulse jets is small, the proportional navigation guidance, as well as the parabolic and proportional navigation guidance control laws, exhibits large mean miss distance. All control laws appear to be equally susceptible to accelerometer and gyroscope errors that corrupt inertial measurement unit rocket state feedback.				
14. SUBJECT TERMS rocket, control, pulse, jet			15. NUMBER OF PAGES 32	
			16. PRICE CODE	
17. SECURITY CLASSIFICATION OF REPORT UNCLASSIFIED	18. SECURITY CLASSIFICATION OF THIS PAGE UNCLASSIFIED	19. SECURITY CLASSIFICATION OF ABSTRACT UNCLASSIFIED	20. LIMITATION OF ABSTRACT UL	

INTENTIONALLY LEFT BLANK.